Transcription precedes loss of *Xist* coating and depletion of H3K27me3 during X-chromosome reprogramming in the mouse inner cell mass

Lucy H. Williams, Sundeep Kalantry*, Joshua Starmer and Terry Magnuson[†]

SUMMARY

Repression of *Xist* RNA expression is considered a prerequisite to reversal of X-chromosome inactivation (XCI) in the mouse inner cell mass (ICM), and reactivation of X-linked genes is thought to follow loss of *Xist* RNA coating and heterochromatic markers of inactivation, such as methylation of histone H3. We analyzed X-chromosome activity in developing ICMs and show that reactivation of gene expression from the inactive-X initiates in the presence of *Xist* coating and H3K27me3. Furthermore, depletion of *Xist* RNA coating through forced upregulation of NANOG does not result in altered reactivation kinetics. Taken together, our observations suggest that in the ICM, X-linked gene transcription and *Xist* coating are uncoupled. These data fundamentally alter our perception of the reactivation process and support the existence of a mechanism to reactivate Xp-linked genes in the ICM that operates independently of loss of *Xist* RNA and H3K27me3 from the imprinted inactive-X.

KEY WORDS: X inactivation, Epigenetic reprogramming, Pre-implantation mouse development

INTRODUCTION

X-chromosome inactivation (XCI) results in the transcriptional silencing of most genes on one of the two X-chromosomes to equalize X-linked gene dosage in female cells with that in XY male cells (Avner and Heard, 2001). Although the exact mechanism for X-linked gene silencing is unknown, XCI requires expression of the long non-coding RNA *X inactive-specific transcript* (*Xist*) (Brown et al., 1991; Marahrens et al., 1997; Penny et al., 1996). *Xist* RNA is expressed from and preferentially coats the inactive X-chromosome (Clemson et al., 1996). *Xist* coating is followed by recruitment of multiple chromatin-modifying complexes, such as the polycomb repressive complex 2 (PRC2), which trimethylates lysine 27 on histone H3 to give H3K27me3 (Plath et al., 2002; Silva et al., 2003). H3K27me3 is a chromatin modification associated with gene repression, and H3K27me3 enrichment on the inactive-X is essential to maintain imprinted paternal-X silencing in extra-embryonic lineages (Kalantry et al., 2006; Simon and Kingston, 2009). Together, *Xist* coating and H3K27me3 are necessary to establish stable and heritable XCI; thus, these epigenetic modifications are considered to be markers of X-linked gene silencing.

Two types of XCI are evident during development of the female mouse embryo. The first type, imprinted XCI, results in exclusive silencing of the paternal X-chromosome (Takagi and Sasaki, 1975; West et al., 1977). By contrast, the second type of XCI is termed random because either maternal-X (Xm) or paternal-X (Xp) can be chosen for silencing (Lyon, 1961). During early mouse embryogenesis, *Xist* expression is first evident at the two-cell stage and occurs exclusively from the Xp (Kay et al., 1993). *Xist* RNA

gradually coats the Xp during pre-implantation development (Huynh and Lee, 2003; Okamoto et al., 2004). By the early blastocyst stage, prior to specification of extra-embryonic and embryonic lineages, *Xist* accumulation on the Xp (Xp-*Xist* coating) is evident in all cells of the embryo (Sheardown et al., 1997). At the late blastocyst stage, when extra-embryonic and embryonic lineages are determined, Xp-*Xist* coating is maintained in the extra-embryonic trophectoderm and primitive endoderm. By contrast, Xp-*Xist* coating is lost in epiblast cells, which define the progenitor cells of the embryo proper (Mak et al., 2004; Okamoto et al., 2004; Sheardown et al., 1997).

Based on patterns of Xp-*Xist* coating in the blastocyst, it is assumed that all cells of the pre-implantation embryo first undergo the imprinted form of XCI and that this imprint is maintained in the extra-embryonic lineages. In the developing ICM, epiblast precursor cells reverse imprinted XCI in order to subsequently initiate random XCI later in development (Mak et al., 2004; Okamoto et al., 2004). However, three recent reports analyzed Xp-linked gene transcription in single cells of pre-implantation embryos. Each report independently confirmed that some degree of Xp-linked gene silencing is evident as early as the four-cell cleavage stage. Yet, despite *Xist* coating the Xp in all cells, Xp-linked gene silencing is not evident in all cells of the blastocyst, indicating that imprinted XCI is incomplete during pre-implantation development (Kalantry et al., 2009; Namekawa et al., 2010; Patrat et al., 2009). Given these results, it is still unclear whether epiblast progenitor cells, which are specified by the blastocyst stage, exhibit imprinted Xp-linked gene silencing.

Here, we utilized RNA fluorescence in situ hybridization (FISH) techniques to measure directly the kinetics of X-linked gene expression, as opposed to chromosome-wide markers of inactivation, in individual nuclei of developing ICMs. We provide evidence that supports previous assumptions that, prior to epiblast specification, ICM cells exhibit imprinted XCI. We also make the surprising observation that reactivation in the ICM occurs earlier than previously indicated by loss of *Xist* coating (Mak et al., 2004; Okamoto et al., 2004). Coincident with specification of the *Nanog-*

Department of Genetics, Carolina Center for Genome Sciences, and Lineberger Comprehensive Cancer Center, University of North Carolina, Chapel Hill, NC 27599-7264, USA.

*Present address: Department of Human Genetics, 1241 E. Catherine St, University of Michigan Medical School, Ann Arbor, MI 48109-5618, USA
†Author for correspondence (trm4@med.unc.edu)

expressing epiblast lineage, but prior to loss of the *Xist* domain and H3K27me3 enrichment on the Xp, mid-stage ICMs exhibit an increase in Xp-linked gene expression, indicative of active transcription. Recent results suggest that pluripotency-associated transcription factors NANOG, OCT3/4 (POU5F1 – Mouse Genome Informatics) and SOX2 might directly regulate X-chromosome activity by preventing upregulation of *Xist* expression in mouse embryonic stem cells (ES cells) (Navarro et al., 2008). We show that forced upregulation of NANOG results in loss of Xp-*Xist* coating without affecting the kinetics of Xp-linked gene reactivation. These observations argue against a direct role for NANOG-dependent *Xist* repression as a requirement for initiation of Xp expression. We present an alternative hypothesis that reversal of imprinted X-chromosome inactivation occurs by separable steps, with gene reactivation being independent from loss of the *Xist* and H3K27me3 domains.

MATERIALS AND METHODS

Embryo collection and immunosurgery
Embryos were collected from natural mating of either *Mus musculus domesticus* CD1 females (RNA FISH) or *Mus musculus molossinus* JF1 females (RT-PCR) to CD1 males carrying the X-GFP (D4.EGFP) transgene (Hadjantonakis et al., 1998). Female blastocysts were distinguished from males by *GFP* expression. The *Grb2*$^{-/-}$ (Grb2tm2Paw) line was described previously (Cheng et al., 1998). Mice were exposed to light daily between 06.00 h and 18.00 h. The morning of the day the plug was detected was considered to be embryonic day (E)0.5. Early blastocysts were collected between E2.75 and E3.0 (~66-72 hours post-copulation). Mid-stage blastocysts were collected between E3.5 and E3.75 (~84-90 hours post-copulation). Because embryos collected at the same time varied in developmental stage, blastocysts were also staged according to size (a measure of total cell number) and blastoceol cavity expansion (see Fig. S6 in the supplementary material). Immunosurgery procedures were performed as described previously (Solter and Knowles, 1975).

Immunostaining
Embryos were fixed in 3% paraformaldehyde for 10 minutes at room temperature. After washing in 1×PBS, embryos were permeabilized in 0.5% Triton X-100 for 15 minutes. Embryos were then washed in 1×PBS and blocked in 10% serum for 1 hour at room temperature. Primary antibodies were: Nanog (Chemicon, 1:1000), Gata6 (R&D Systems, 1:1000), H3K27me3 (Upstate, 1:250) and EED (Arie Otte, Slater Institute, The Netherlands, 1:200). Primary antibody incubations were performed overnight at 4°C. Embryos were washed in 1×PBS and incubated in secondary antibody for 45 minutes at room temperature. Secondary antibodies coupled to Alexa Flour 594 (Invitrogen A-11037) and Alexa Fluor 488 (Invitrogen A-11039) were diluted to 1:500. The embryos were washed in 1×PBS and mounted into 0.12 mm deep Secure-Seal spacer wells (Invitrogen, S24737) on microscope slides in Vectashield (Vector Labs) diluted 1:1 with DAPI.

RNA FISH
FISH probes were generated from BAC and FOSMID clones (BACPAC Resources Center, CA, USA) and labeled using the Bioprime Labeling Kit (Invitrogen) with FITC-dUTP (Roche), Cy3-dCTP (GE Healthcare) or Cy5-dCTP (GE Healthcare). FOSMIDs and BACs used were: *G135P65743A11* (*Ube1x*), *G135P69277C4* (*Mecp2*), *G135P63425C4* (*Xist/Tsix*), *G135P605237C7* (*Rnf12*), *RP24-274B9* (*Abcb7*), *G135P603627A9* (*Smcx*), *G135P60684B7* (*Nanog*) and *RP24329F11* (*Gata6*). Two FOSMIDs *G135P62497G3* and *G135P64951A11* were used to detect *Atp7a*. Mouse Cot-1 DNA (Invitrogen) was used in the Cot-1 RNA FISH experiments. RNA FISH was performed as described previously (Kalantry et al., 2009). All RNA FISH probes used to detect X-linked genes were tested in trophoblast (TS) and embryonic stem (ES) cell lines to determine detection of X-linked sequences with expected expression patterns. *Nanog* and *Gata6* FISH probes were tested in ES and

extra-embryonic endoderm (XEN) cell lines, respectively. For combined immunostaining of H3K27me3 and RNA FISH, RNA FISH was performed after immunostaining.

Statistical analysis of RNA FISH
RNA FISH nuclei were classified as biallelic, monoallelic or nonscorable. Nuclei were classified as nonscorable when no signal could be detected. For each X-linked gene, the total number of the three classes of nuclei was compared between early and mid-stage ICMs. Binomial exact test was used to verify that nonscorable data between stages were equivalent. Fisher's exact test compared the three categories between early and mid-stage ICMs. *P* values <0.01 were considered to be statistically significant. The procedure was repeated for the Cot-1 RNA FISH experiments except nuclei were scored as either excluded, overlapping or nonscorable.

Microscopy
Images for RNA FISH were obtained using a Leica DML fluorescence microscope with a Q-imaging Retiga 200R camera and Q-capture software. Images were processed using SPOT RT Software (Diagnostic Instruments). For Cot-1 RNA FISH and immunostaining, a Zeiss710 confocal microscope was used. Confocal sections were analyzed using Zen software to determine overlap between signals. To determine relative intensity values obtained in the Cot-1 RNA experiments, we generated line traces across nuclei using NIH Image J software and used the plot profile tool to measure the intensity across the line traces.

RT-PCR
RT-PCR was performed as described previously (Kalantry et al., 2009). In brief, mRNA was prepped using the Dynabeads mRNA DIRECT Micro Kit (Invitrogen, 610.21). ICMs were lysed in 100 µl of lysis/binding buffer. For RT-PCR, SuperScript III One-Step RT-PCR Platinum Taq (Invitrogen, 12574-035) was used to amplify the cDNA. A portion of the final RT-PCR product was used to perform one round of amplification in the presence of a trace amount of ^{32}P-dCTP (Perkin Elmer, BLU513H). The final PCR product was digested with the appropriate restriction enzyme, run on a 10% acrylamide gel and exposed to film. All RT-PCR primers were described previously (Kalantry et al., 2009). Band intensities were quantified using Adobe Photoshop CS3 Extended software. Percent paternal expression was calculated as a percentage of total intensity of combined maternal- and paternal-specific bands, i.e. % Xp = [Xp/(Xm+Xp)]×100. In the case of multiple maternal- or paternal-specific bands, the band intensities were added to yield a single value. The average % Xp was compared between early and mid-stage ICMs. *P*-values were calculated using two-tailed *t*-tests where the null hypothesis is that the mean % Xp of early and mid-stage samples are the same.

RESULTS

Imprinted XCI is established in early ICMs prior to epiblast specification
To investigate Xp activity in the ICM, we analyzed transcription of X-linked genes by RNA FISH in ICMs isolated by immunosurgery (Solter and Knowles, 1975). We assayed five X-linked genes [*Rnf12* (*Rlim* – Mouse Genome Informatics), *Atp7a*, *Abcb7*, *Ube1x* (*Uba1* – Mouse Genome Informatics) and *Mecp2*] that are expressed at robust levels during the cleavage stages of pre-implantation development (Kalantry et al., 2009; Patrat et al., 2009). Previous allele-specific RT-PCR and RNA FISH data showed a bias towards Xm expression of these genes at the morula stage, indicating that these genes are subject to imprinted XCI (Huynh and Lee, 2003; Kalantry et al., 2009). We assayed expression of the five X-linked genes together with *Xist* RNA, which marks the Xp, in ICMs of early stage blastocysts (~32-cell stage embryo) (Fig. 1A). If the Xp-allele of the five genes assayed is silenced, RNA FISH will yield a single monoallelic gene signal indicative of transcription from the Xm. If the Xp-linked gene is not silenced, our assay will detect gene expression from both X-
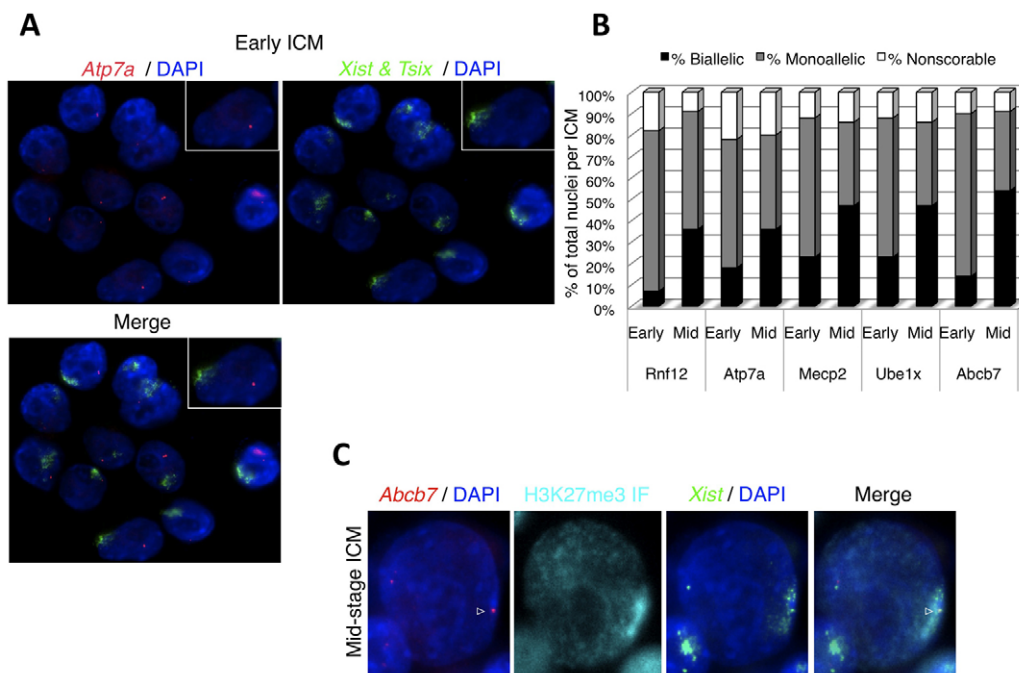
Fig. 1. Mid-stage inner cell masses (ICMs) exhibit increasing Xp-linked gene expression. (**A**) A representative ICM assayed for *Atp7a* (red, left panel) and *Xist* and *Tsix* (green, right panel) by RNA fluorescence in situ hybridization (FISH). The *Xist* probe detects *Xist* RNA and the anti-sense transcript detects *Tsix*. *Xist* marks the Xp as a cloud at this stage. In ICMs, *Tsix* is detected in some nuclei as a pinpoint signal from the Xm (Lee et al., 1999). In the merge image, all nuclei exhibit monoallelic *Atp7a* expression, localized away from the Xp-*Xist* coat (green domains). A single nucleus is highlighted in the right corner of each image. (**B**) Distributions of biallelic (black), monoallelic (gray) and nonscorable (white) nuclei are presented as the average percentage of nuclei per early or mid-stage ICM. In mid-stage ICMs there is a statistically significant ($P<0.01$) increase in biallelism and decrease in monoallelism compared with early stage ICMs. (**C**) A representative nucleus illustrates biallelic *Abcb7* (red, first panel) expression. H3K27me3 accumulates on the Xp above genomic levels (cyan, second panel). The H3K27me3 enrichment domain colocalizes with Xp-*Xist* coating (green cloud, third panel). The merge image (fourth panel) indicates that one of the two *Abcb7* RNA FISH signals (marked by an arrowhead) colocalizes with both the Xp *Xist* and H3K27me3 domains. Nuclei are stained with DAPI.

chromosomes. As a positive control, we measured expression of *Smcx* (*Kdm5c* – Mouse Genome Informatics), a gene known to escape imprinted XCI (Agulnik et al., 1994; Plusa et al., 2008). As expected, *Smcx* exhibited 97% biallelic expression in cells of early ICMs, demonstrating that our assay is capable of detecting biallelic X-linked gene transcription (see Fig. S1A in the supplementary material). By contrast, *Rnf12*, *Atp7a*, *Abcb7*, *Ube1x* and *Mecp2* demonstrated an average low level of biallelism, ranging from 5% to 23% of cells per ICM (Fig. 1B). This low level of biallelism is comparable to the level of biallelism in trophectoderm nuclei (see Fig. S1B in the supplementary material). A majority (60%) of all early ICMs analyzed exhibited either one or no biallelic nuclei, and a number of individual ICMs exhibited exclusive (100%) monoallelic *Rnf12*, *Atp7a*, *Abcb7* and *Ube1x* expression in every nucleus. Together, these data argue against the possibility that escape from imprinted XCI is a general characteristic of ICM nuclei and suggest that early ICMs undergo Xp silencing to the same degree as do cells of the trophectoderm. Therefore, the majority of nuclei in the pre-implantation embryo exhibit Xp-linked gene silencing and undergo imprinted XCI prior to specification of the embryonic lineage.

Xp reactivation occurs in the presence of the Xp-*Xist* domain

Reactivation of the Xp has been described to occur in the epiblast of late (fully expanded or hatched) blastocysts (~128-cell stage embryo) after the sequential loss of *Xist* coating, the PRC2 subunit

EED, and H3K27me3 on the Xp (Mak et al., 2004; Okamoto et al., 2004; Silva et al., 2009). To investigate the timing of Xp reactivation, we isolated ICMs from mid-stage female blastocysts (~32- to 64-cell stage embryo). We first performed dual immunofluorescence to detect NANOG, which marks the ICM, and EED in mid-stage blastocysts. On average, 90% of NANOG positive nuclei exhibited an EED Xp domain (Mak et al., 2004; Okamoto et al., 2004; Silva et al., 2009) (see Fig. S2A in the supplementary material). Xp EED domains in ICM nuclei also exhibited accumulation of H3K27me3 (see Fig. S2B in the supplementary material). As H3K27me3 is a hallmark of transcriptionally inactive chromatin domains, these data imply Xp-linked genes are inactive in mid-stage ICMs. We next investigated the transcriptional status of the Xp-linked genes directly using RNA FISH. Assaying the same five X-linked genes that previously showed predominantly monoallelic expression in early ICMs, we detected biallelic expression in 35-50% of cells from mid-stage ICMs (Fig. 1B). Importantly, in all cases of biallelism one of the two X-linked gene signals colocalized with Xp-*Xist* and H3K27me3 accumulation, and the percentage of nuclei exhibiting Xp-*Xist* coating did not change significantly (Fig. 1C; see Fig. S2C in the supplementary material). In contrast to early ICMs, we never observed a mid-stage ICM that exhibited 100% monoallelic nuclei. For all five X-linked genes analyzed, we observed a statistically significant increase in biallelism and a corresponding decrease in monoallelism ($P<0.01$; Fig. 1B; see Table S1 in the supplementary material). Given the cell division timing (~11.5 hours) of ICM
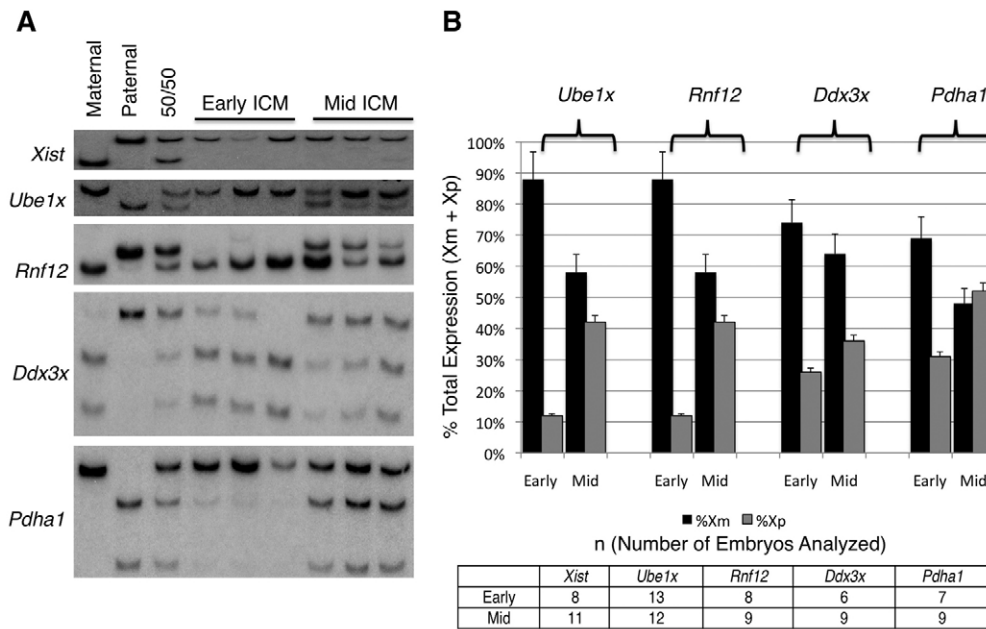
Fig. 2. Dynamics of X-linked gene expression assayed by allele-specific RT-PCR. F1 hybrid mouse embryos were generated by mating JF1 females to CD1 males. Xm and Xp transcripts were distinguished utilizing single nucleotide polymorphisms between the two strains. (**A**) Allele-specific expression was analyzed for *Xist* and the X-linked genes *Ube1x*, *Rnf12*, *Pdha1* and *Ddx3x*. Lane 1, Xm allele; Lane 2, Xp allele; Lane 3, equal amounts of Xm and Xp allele; Lanes 4-6, early F1 hybrid inner cell mass (ICM) samples; Lanes 7-9, mid-stage F1 hybrid ICM samples. Analysis of *Xist* expression illustrates that in both early and mid-stage ICMs, *Xist* is expressed from the Xp. In early ICMs, X-linked gene expression for *Ube1x*, *Rnf12*, *Pdha1* and *Ddx3x* is largely from the Xm allele. In mid-stage ICMs there is increasing Xp expression of Xp-linked genes. (**B**) Average Xm and Xp contributions were calculated as a percentage of total expression (Xm+Xp). There is a statistically significant increase in average Xp expression in mid-stage ICMs compared with early stage ICMs for each X-linked gene analyzed ($P<0.01$). The number of ICMs examined is presented in the table.

nuclei and the low level of biallelism detected at the early stage, it is also unlikely that escape from imprinted XCI, for any of the genes assayed, can account for the increase in biallelic nuclei (Bischoff et al., 2008). These data suggest that reactivation of genic transcription occurs earlier than determined previously by analysis of inactive-X epigenetic markers and, remarkably, occurs in the presence of Xp-*Xist* coating and H3K27me3 accumulation on the Xp.

To confirm our RNA FISH results, we analyzed allele-specific X-linked gene expression using RT-PCR in individual ICMs obtained from crosses between *M. domesticus* (CD1) and *M. molossinus* (JF1) strains. We first measured expression of *Xist* RNA. In early F1 ICMs, *Xist* transcription was detectable exclusively from the Xp (Fig. 2A). At mid-stage, *Xist* transcription was maintained on the Xp (Fig. 2A) consistent with Xp-*Xist* coating, which was evident by RNA FISH (Fig. 1C). We next quantified the expression of maternal and paternal alleles for four X-linked genes (*Ube1x*, *Rnf12*, *Ddx3x* and *Pdha1*), which were previously shown to exhibit imprinted Xp silencing in extra-embryonic tissues (Kalantry et al., 2009). All four X-linked genes exhibited biased Xm expression in early ICMs (Fig. 2A). For *Ube1x* and *Rnf12*, very little Xp expression could be detected in early ICMs. Paternal silencing of *Pdha1* and *Ddx3x* was less complete but still favored expression from the Xm. These data agree with our RNA FISH results and verify that imprinted XCI is present in early stage ICMs. By contrast, when individual mid-stage ICMs were analyzed, robust expression from the paternal allele was detected (Fig. 2A). *Ube1x*, *Rnf12*, *Pdha1* and *Ddx3x* all exhibited a statistically significant increase in paternal X-linked gene expression in mid-stage compared with early ICMs ($P<0.05$;

Fig. 2B; see Table S2 in the supplementary material). These data illustrate the detection of not only nascent transcripts but also spliced polyadenylated transcripts, confirming an increase in Xp-linked gene expression in mid-stage ICMs.

Together, our RNA FISH and allele-specific RT-PCR results show that reactivation of seven Xp-linked genes occurs in the presence of Xp-*Xist* coating. In order to determine the broader transcriptional status of the Xp, we next hybridized with a Cot-1 DNA probe and *Xist* probe in our RNA FISH experiments. Under RNA FISH conditions, Cot-1 DNA hybridizes to transcribed repetitive sequences of the genome (Hall et al., 2002). In combination with a *Xist* probe, Cot-1 RNA FISH allows visualization of general transcription within the *Xist* RNA domain. It has previously been shown that the X-chromosome is devoid of Cot-1 hybridization when gene silencing is established (Chaumeil et al., 2006; Namekawa et al., 2010). Consistent with predominant Xp-silencing, we detected mutually exclusive *Xist* and Cot-1 RNA FISH signals in the majority (~82%) of trophectoderm nuclei of mid-stage blastocysts (Fig. 3A). By contrast, when we performed RNA FISH on mid-stage ICMs, we detected nuclei with overlap of Cot-1 and *Xist* RNA FISH signals (Fig. 3B; see Fig. S3 in the supplementary material). Cot-1 RNA FISH signal typically overlapped the exterior of the intense *Xist* domain, although nuclei were also detected that exhibited an Xp-*Xist* domain that completely overlapped with the Cot-1 RNA FISH signal (see Fig. S3 in the supplementary material). We quantified the number of nuclei per mid-stage ICM that exhibited patterns of mutually exclusive or overlapping RNA FISH signals (Fig. 3A). On average, 45% of nuclei per mid-stage ICM exhibited overlapping signals of Cot-1 and *Xist*. Compared with the trophectoderm, the ICM is,
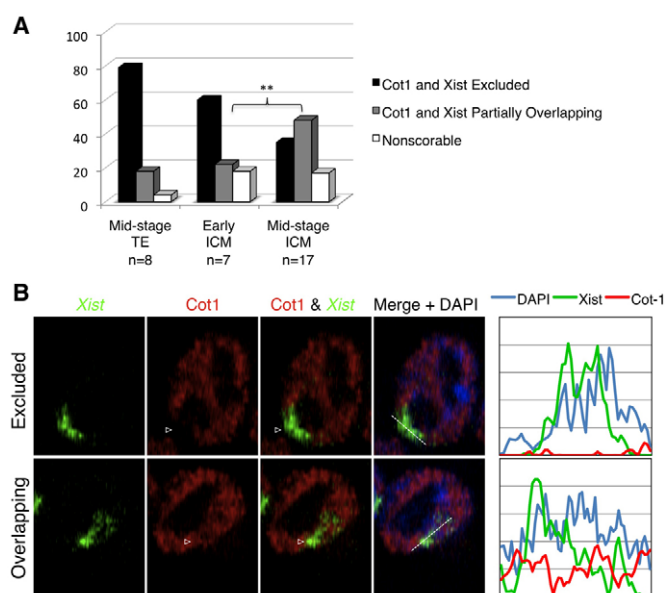
Fig. 3. Mid-stage inner cell masses (ICMs) exhibit transcription within the Xp-*Xist* domain. Cot-1 DNA (red) and *Xist* (green) probes were used in RNA FISH experiments to determine general Xp transcriptional status. (**A**) The average distribution of nuclei with mutually excluded or overlapping Cot-1 and *Xist* RNA FISH signals are shown as a percentage of total nuclei per mid-stage trophectoderm (TE), early ICM and mid-stage ICM. The bracket represents a statistically significant (*P<XXXX*) increase in the percentage of cells exhibiting overlapping FISH signals in mid-ICMs compared with early-ICMs. (**B**) Representative mid-stage ICM nuclei indicate mutually excluded or overlapping patterns. Arrowheads indicate the *Xist* domain. Dashed lines indicate the area of the merged figure represented in the line scans. Line scans indicate the relative intensities of DAPI, Cot-1 and *Xist* signals.

therefore, enriched with nuclei exhibiting Cot-1 signal overlapping the Xp-*Xist* domain (Fig. 3A). This pattern of overlap is not simply characteristic of ICM cells, in general, as we detected a significant (*P*<0.01) increase in the number of nuclei with overlap when we compared early to mid-ICMs (Fig. 3A). This increase in the number of nuclei exhibiting transcription from within the *Xist* RNA domain is consistent with general Xp reactivation occurring in the presence of *Xist* coating. In combination with our previous gene-by-gene RNA FISH (Fig. 1B) and allele-specific RT-PCR results (Fig. 2B), these data suggest that the presence of *Xist* coating and the accumulation of PRC2 and H3K27me3 are not sufficient for X-chromosome silencing.

The mid-stage ICM is composed of cells specified to both epiblast and primitive endoderm (Chazaud et al., 2006). Thus, we next investigated whether the biallelic gene expression evident in mid-stage ICMs corresponded to the epiblast cell fate. Cell fate in the maturing ICM is adopted from mutually exclusive expression of lineage markers *Nanog* (epiblast) and *Gata6* (primitive endoderm), which is resolved from uniform expression of these markers in the early ICM. We analyzed NANOG and GATA6 in mid-stage blastocysts (see Fig. S4A in the supplementary material). As previously reported, at mid-stage NANOG and GATA6 were not expressed mutually exclusively in the ICM (Plusa et al., 2008). However, we reasoned that changes in protein products might lag behind changes in gene expression; consequently, analysis of primary transcripts by RNA FISH might confer a more accurate

expression pattern of *Nanog* and *Gata6* to be utilized for lineage markers. We found that *Nanog* and *Gata6* nascent transcripts in mid-stage ICMs were largely detected as mutually exclusive cell populations (see Fig. S4B in the supplementary material). On average, ~47% of cells per ICM exhibited exclusive *Nanog* expression. By contrast, ~32% of cells exhibited exclusive *Gata6* expression. On average, 21% of cells per ICM co-expressed both lineage markers (see Fig. S4B in the supplementary material). The degree of mutually exclusive lineage marker expression appears to depend upon the maturity of the blastocyst with more developed blastocysts exhibiting fewer cells with co-expression. These data correspond to predicted patterns of *Nanog* and *Gata6* expression, based primarily on protein localization at later stages of ICM development, and validate the use of RNA FISH to measure *Nanog* expression in mid-stage ICMs (Plusa et al., 2008).

Restriction of *Nanog* expression to epiblast progenitors appeared to be more complete in further developed mid-stage blastocysts. Therefore, in the following experiments, we limited our assays to isolated ICMs from blastocysts of ~58-64 cells. In these ICMs, we assayed *Nanog* expression in cells that exhibited biallelic expression of X-linked genes *Atp7a* and *Mecp2*. We found that most cells expressing *Atp7a* and *Mecp2* from both X-chromosomes also expressed *Nanog* (Fig. 4A; see Fig. S4C in the supplementary material). The reverse was true for *Gata6* expression, which, when assayed in independent experiments, was rarely detected in cells exhibiting biallelic X-linked gene expression (see Fig. S4D in the supplementary material). We also show that in biallelic mid-stage *Nanog*-positive cells, *Xist* clearly coated the Xp (Fig. 4B,C). Utilizing *Nanog* as an epiblast specific marker, we located the cells exhibiting biallelic X-linked gene expression to the epiblast progenitor population. Biallelic gene expression is, therefore, biased to the epiblast cell fate and not simply a function of incomplete Xp silencing during pre-implantation development. We conclude that Xp expression in mid-stage ICMs is a result of reversing imprinted XCI.

Ectopic extinction of the *Xist* coat has no affect on Xp-linked gene reactivation

The prevailing hypothesis suggests that reactivation of X-linked genes in the ICM results from *Xist* RNA downregulation. These data are supported by evidence that *Xist* RNA coating is lost in the late stage ICM (Mak et al., 2004; Okamoto et al., 2004). However, the data presented thus far argue against loss of the *Xist* coat as a prerequisite to initiate Xp genic reactivation. One possibility that might explain reactivation of X-linked genes in the presence of *Xist* coating is that *Xist* expression gradually decreases as the ICM develops. If so, nuclei exhibiting biallelic X-linked gene expression might represent nuclei with lower levels of *Xist* coating. Thus, Xp-linked gene reactivation could be triggered by decreasing amounts of *Xist* coating, which would support the previous hypothesis that loss of *Xist* triggers reactivation. Such subtle decreases in amount of *Xist* transcripts coating the Xp might also be undetectable by RNA FISH. In order to address this possibility, we sought to deplete *Xist* coating in mid-stage ICMs. We reasoned that if Xp gene expression were regulated independently of *Xist* coating then precocious loss of the Xp-*Xist* domain would have no effect on the kinetics of genic reactivation. By contrast, if decreasing levels of *Xist* trigger reactivation, then dramatic loss of *Xist* should result in reactivation of the Xp.

For these experiments, we took advantage of a genetic mutation in *Grb2*, a key adaptor molecule necessary for MAP kinase signal transduction, which has been shown to regulate *Nanog* expression
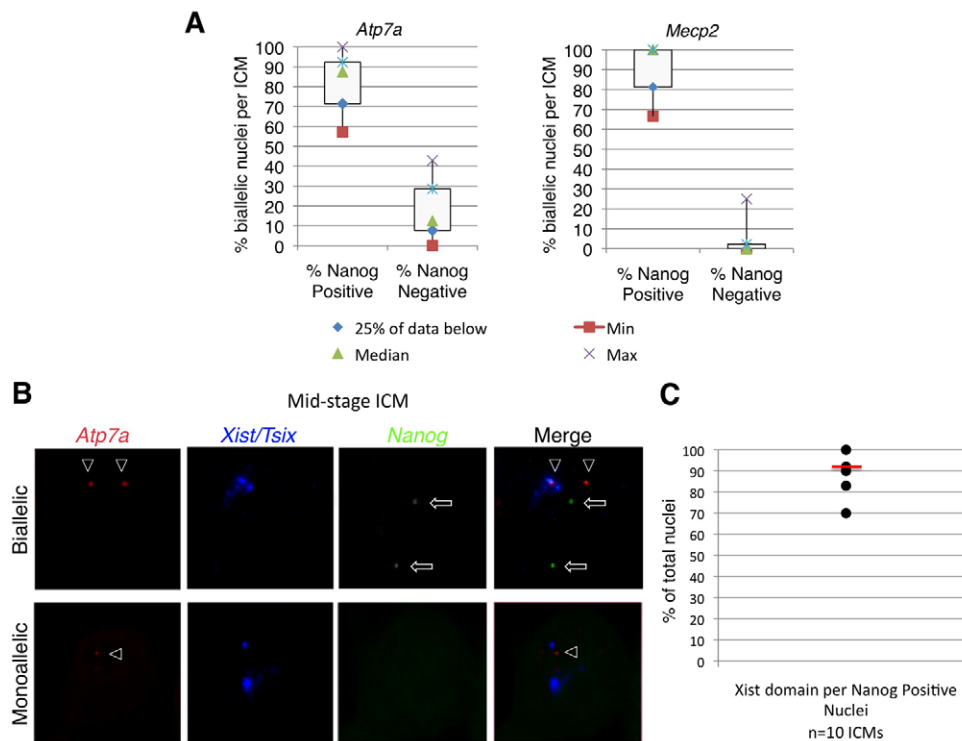
Fig. 4. *Nanog* expression corresponds to biallelic X-linked gene expression in mid-stage inner cell masses (ICMs). (**A**) Side-by-side box plots graphically represent the percentage of biallelic nuclei (*y*-axis) grouped as either positive or negative for *Nanog* transcripts (*x*-axis). The box plot on the left represents ICMs assayed for *Atp7a* expression and the right-hand box plot represents ICMs assayed for *Mecp2* expression. The medians of the data are indicated (green triangle). The boxes contain the middle 50% of the data. Whiskers represent maximum and minimum values of the dataset. The box plots are nonoverlapping, illustrating that the population of biallelic nuclei are largely skewed towards being *Nanog* positive. (**B**) Representative nuclei of a mid-stage ICM showing detection of *Atp7a* (red), *Xist* RNA (blue) and *Nanog* (green) assayed by RNA FISH. Top row: Biallelic *Atp7a* (red) expression is marked by arrowheads (first panel) with one allele overlapping *Xist* transcripts (blue, second panel). *Nanog* transcripts (green) are marked by arrows (third panel). Bottom row: Monoallelic *Atp7a* expression is marked by an arrowhead (first panel) and colocalizes with *Tsix* expression (blue pinpoint signal, second panel) from the Xm. In this nucleus, *Nanog* is not expressed (third panel). (**C**) The graph represents the distribution of the percentage of nuclei from mid-stage *Nanog* positive nuclei that exhibit Xp-*Xist* coating. The red line represents the average. *n*, the number of embryos analyzed.

(Hamazaki et al., 2006; Pawson and Scott, 1997). NANOG expression was highly variable in the mid-stage ICM, with strong NANOG immunostaining detectable in only a subset of ICM cells (Fig. 5A; see Fig. S4A in the supplementary material). By contrast, *Grb2*⁻/⁻ blastocysts exhibited strong NANOG immunostaining in the majority of ICM cells (Fig. 5A) (Chazaud et al., 2006). It has been reported that NANOG directly represses *Xist* expression in undifferentiated mouse ES cells (Navarro et al., 2008). In support of these results, upregulation of *Nanog* due to inhibition of MAPK/ERK signaling resulted in loss of the Xp EED domain in all ICM cells at E4.5 (Nichols et al., 2009). We also observed that female mid-stage E3.5 *Grb2*⁻/⁻ blastocysts exhibited uniform loss of EED and H3K27me3 Xp enrichment specifically in the ICM (Fig. 5A; see Fig. S5 in the supplementary material). Trophectoderm cells appeared to maintain both inactive-X markers in wild-type and *Grb2*⁻/⁻ blastocysts (Fig. 5A; see Fig. S5 in the supplementary material). We also found a significant reduction in the number of ICM cells with Xp-*Xist* coating in *Grb2*⁻/⁻ ICMs compared with littermate controls (Fig. 5B). This was in contrast to *Grb2*⁻/⁻ embryos isolated between the 8- and 16-cell stage, which exhibited normal initiation of Xp silencing and Xp-*Xist* coating. In addition, we noted that even when Xp-*Xist* coating was detectable in *Grb2*⁻/⁻ mid-stage ICMs, the density of the coat was significantly reduced (Fig. 5C). Importantly, when we analyzed

Xp-linked gene activity, we found similar patterns of monoallelic and biallelic Xp-linked gene expression in female *Grb2*⁻/⁻ ICMs compared with female littermate controls, irrespective of the amount of *Xist* coating the Xp (Fig. 5C). In fact, for the four genes we analyzed (*Ube1x*, *Rnf12*, *Atp7a* and *Abcb7*) monoallelic X-linked gene expression was detectable in cells without visible Xp-*Xist* coating (Fig. 5B,C). Despite widespread loss of Xp-*Xist* and Xp-EED accumulation, reactivation in *Grb2*⁻/⁻ ICMs occurs normally. Analysis of ICM nuclei from late-stage blastocysts (~128 cells) also indicates that in the absence of *Xist* coating, Xp silencing can be maintained through cell divisions (data not shown). These data rule out the possibility that the reactivation detected in the mid-stage ICM is due to subtle decreases in the levels of *Xist* and show that genic silencing in the ICM can be maintained independently of cytologically detectable *Xist* coating.

DISCUSSION
Here, we present evidence that reversal of imprinted XCI, as evident by an increase in Xp-linked gene activity, initiates in the mid-stage ICM coincident with specification of the epiblast progenitor population. Genic reactivation occurs in the presence of *Xist* coating, as well as the cytologically detectable PRC2 and H3K27me3 domains. Together, these observations suggest that, particularly at this early stage of embryonic development, these
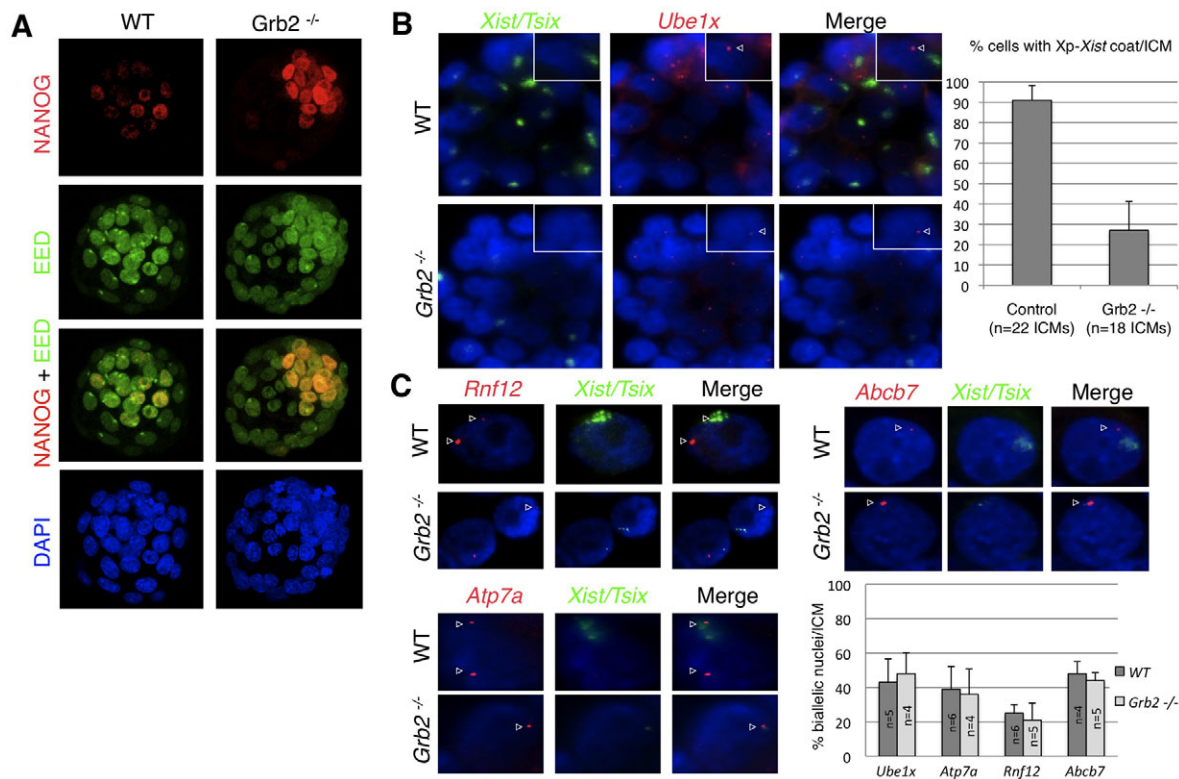
Fig. 5. *Grb2⁻/⁻* inner cell mass (ICM) cells exhibit loss of *Xist* transcripts and EED on the Xp. (A) Mid-stage blastocysts immunostained for NANOG (red, top row) and EED (green, second row). NANOG marks the epiblast progenitors. In wild-type blastocysts (left panels), EED accumulates on the Xp in NANOG positive nuclei as seen by the green foci (merge, third row). However, in all but one NANOG positive nuclei of *Grb2⁻/⁻* blastocysts (right-hand panels), Xp EED foci are undetectable (merge, third row). DAPI (blue, fourth row) stains all nuclei. **(B)** Wild-type (WT, top row) and *Grb2⁻/⁻* (bottom row) mid-stage ICMs assayed by RNA FISH for transcripts of *Xist/Tsix* (green, left-hand panels) and *Ube1x* (red, middle panels). *Grb2⁻/⁻* ICMs exhibit a decrease in Xp-*Xist* coating (green, left panel). A representative nucleus is highlighted and an arrowhead marks monoallelic *Ube1x* expression, which occurs despite the absence of Xp-*Xist* coating. The graph indicates the average percentage of cells per ICM that exhibit *Xist* coating in *Grb2⁻/⁻* compared with wild-type littermate controls. Error bars represent xxx. **(C)** Nuclei from wild-type (upper rows) and *Grb2⁻/⁻* (bottom rows) ICMs assayed for transcripts of X-linked genes *Rnf12*, *Atp7a* and *Abcb7* (red signals marked by arrowheads, left panels) and *Xist/Tsix* (green, middle panels). *Grb2⁻/⁻* ICM nuclei (bottom rows) show monoallelic expression in the absence of the Xp-*Xist* domain (merge, right panels). The graph indicates the distribution of biallelic X-linked gene expression in *Grb2⁻/⁻* ICMs compared with wild type. The data are presented as a percentage of total cells per ICM. Error bars represent s.d.

epigenetic marks, classically analyzed at the cytological level to generalize X-chromosome activity, do not accurately reflect the expression state of individual X-linked genes.

In addition, we argue that genic reactivation is not simply a consequence of loss of *Xist* coating. We present evidence that X-linked gene silencing, at least for a subset of genes, can be maintained even after *Xist* coating and PRC2 accumulation are removed from the Xp. These data appear to be fundamentally at odds with the prevailing mechanism for X-chromosome reactivation, which suggests that reactivation initiates owing to loss of these epigenetic modifications.

It has long been thought that gene silencing occurs first at X-linked genes located nearest the *Xist* locus, extends linearly to distant regions of the X-chromosome, and depends on the spread of *Xist* coating (Huynh and Lee, 2003). The ability to analyze imprinted Xp silencing at the level of single cells has now revealed diverse silencing kinetics between genes and no correlation between the proximity to *Xist* and the speed or efficiency of silencing could be made (Patrat et al., 2009). Although our study analyzes a subset of X-linked genes, the proximity to *Xist* had no consequence in the propensity to reactivate. The seven X-linked

genes analyzed were chosen at random and are located along the length of the X-chromosome, yet all genes exhibited reactivation in the presence of *Xist* or PRC2 accumulation. We argue it is unlikely that these genes represent a subset of X-linked genes that exhibit a propensity to reactivate.

Recent data have shown that *Xist* transcripts first concentrate near the *Xist* locus, located within the X-chromosome inactivation center (XIC), and then coating spreads to the rest of the chromosome (Sarma et al., 2010); however, how spreading occurs is poorly understood. It is possible that *Xist* does not coat the entire X-chromosome in a linear fashion. *Xist* transcripts might favor certain DNA sequences defined as booster elements (Gartler and Riggs, 1983). *Xist* transcripts can associate with autosomal DNA sequences, suggesting that *Xist* coating is not dependent on unique X-linked gene sequences. This led to the hypothesis that repetitive sequences might function as booster elements (Lyon, 1998). A possible explanation for ICM reactivation in the presence of *Xist* coating is that, even though *Xist*, PRC2 and H3K27me3 are detected cytologically accumulating on the Xp, the spread of these epigenetic modifications could be incomplete. In both early and mid-stage ICMs, *Xist* coating and PRC2 and H3K27me3 might not have

reached all genic loci. In the absence of epigenetic modifications at individual loci, there exists no block to prevent gene specific reactivation from occurring prior to the chromosome-wide removal of epigenetic modifications. Owing to the small number of cells and heterogeneity in the developing ICM, we are limited to cytological detection of these epigenetic modifications, which is low resolution compared with the level of DNA sequence. In the future, analysis of *Xist* coating and chromatin modifications at high resolution might allow us to determine how these modifications spread to genic loci during pre-implantation development.

The inactive-X in interphase nuclei is organized into a unique heterochromatic structure referred to as the Barr body (Barr and Carr, 1962). The Barr body can be detected cytologically as a RNA polymerase II-depleted domain, with X-linked genes positioned on the outer rim of an interior core composed primarily of repetitive non-coding sequences (Chaumeil et al., 2006; Clemson et al., 2006). Examination of XCI kinetics suggests that formation of the silent, repetitive non-coding core occurs prior to X-linked gene silencing (Chaumeil et al., 2006; Namekawa et al., 2010). Thus, it has been proposed that repression of repetitive non-coding sequences might contribute to X-linked gene silencing by facilitating packaging of the inactive-X into the RNA polymerase II-depleted Barr body. Formation of the silent repetitive non-coding core also appears to coincide with *Xist* RNA spreading (Chaumeil et al., 2006). However, recent data suggest that during imprinted XCI, repetitive element silencing is initiated independently of *Xist* coating (Namekawa et al., 2010). Based on our observations that Xp reactivation is uncoupled from *Xist* coating, we propose that Xp-linked genes reactivate as a consequence of diminished repeat element silencing, which results in breakdown of the silent inactive-X core and inclusion of transcriptional machinery to the imprinted Xp. In support of our hypothesis, we report that mid-stage ICMs are enriched, relative to trophectoderm and early ICMs, with nuclei exhibiting Cot-1 hybridization internal to the *Xist* domain, suggesting repetitive sequences, within both coding and non-coding sequences, exhibit reactivation prior to removal of *Xist* coating. These data lead us to hypothesize that during pre-implantation development, imprinted Xp-linked gene silencing might be more dependent on general exclusion of the transcriptional machinery from the Xp than on recruitment of *Xist*-dependent heterochromatin modifications.

In conclusion, we have presented a detailed analysis of X-chromosome reactivation kinetics in vivo. Taken together, our data lead us to propose a novel explanation for the reversibility of imprinted XCI in the ICM. We suggest that reprogramming requires two separable events. The first step, relief of Xp-linked gene repression, occurs concomitant with loss of repeat element silencing, between the early and mid-stage of ICM development, and results in two active Xs at the mid-stage. The second step, extinction of Xp-*Xist* coating, occurs in late-stage ICMs by reprogramming of the Xp-*Xist* locus to suppress Xp-*Xist* expression. Together, Xp reactivation and *Xist* reprogramming reset both X-chromosomes for initiation of random XCI in the epiblast. Interestingly, *Xist*-independent imprinted XCI is evident in marsupials in both extra-embryonic and embryonic tissues (Duret et al., 2006; Rens et al., 2010). By separating Xp genic reactivation from *Xist* coating, our data highlight *Xist*-independent mechanisms also occurring in the mouse embryo. How these mechanisms affect characteristics of the inactive-X, such as condensed chromosome structure, depletion of transcriptional machinery, and nuclear organization, to cooperate with *Xist* in mediating X-linked gene silencing is an important question for future studies.

Author contributions
L.H.W., S.K. and T.M. conceived the study and designed the experimental strategy. L.H.W. conducted the experiments. L.H.W., S.K. and T.M. analyzed the data with support from J.S. for statistical analysis of the RNA FISH data. L.H.W. wrote the paper; S.K., J.S. and T.M. edited the paper. All authors discussed the results and commented on the manuscript.

References
Agulnik, A. I., Mitchell, M. J., Mattei, M. G., Borsani, G., Avner, P. A., Lerner, J. L. and Bishop, C. E. (1994). A novel X gene with a widely transcribed Y-linked homologue escapes X-inactivation in mouse and human. *Hum. Mol. Genet.* **3**, 879-884.

Avner, P. and Heard, E. (2001). X-chromosome inactivation: counting, choice and initiation. *Nat. Rev. Genet.* **2**, 59-67.

Barr, M. L. and Carr, D. H. (1962). Correlations between sex chromatin and sex chromosomes. *Acta Cytol.* **6**, 34-45.

Bischoff, M., Parfitt, D. E. and Zernicka-Goetz, M. (2008). Formation of the embryonic-abembryonic axis of the mouse blastocyst: relationships between orientation of early cleavage divisions and pattern of symmetric/asymmetric divisions. *Development* **135**, 953-962.

Brown, C. J., Ballabio, A., Rupert, J. L., Lafreniere, R. G., Grompe, M., Tonlorenzi, R. and Willard, H. F. (1991). A gene from the region of the human X inactivation centre is expressed exclusively from the inactive X chromosome. *Nature* **349**, 38-44.

Chaumeil, J., Le Baccon, P., Wutz, A. and Heard, E. (2006). A novel role for Xist RNA in the formation of a repressive nuclear compartment into which genes are recruited when silenced. *Genes Dev.* **20**, 2223-2237.

Chazaud, C., Yamanaka, Y., Pawson, T. and Rossant, J. (2006). Early lineage segregation between epiblast and primitive endoderm in mouse blastocysts through the Grb2-MAPK pathway. *Dev. Cell* **10**, 615-624.

Cheng, A. M., Saxton, T. M., Sakai, R., Kulkarni, S., Mbamalu, G., Vogel, W., Tortorice, C. G., Cardiff, R. D., Cross, J. C., Muller, W. J. et al. (1998). Mammalian Grb2 regulates multiple steps in embryonic development and malignant transformation. *Cell* **95**, 793-803.

Clemson, C. M., McNeil, J. A., Willard, H. F. and Lawrence, J. B. (1996). XIST RNA paints the inactive X chromosome at interphase: evidence for a novel RNA involved in nuclear/chromosome structure. *J. Cell Biol.* **132**, 259-275.

Clemson, C. M., Hall, L. L., Byron, M., McNeil, J. and Lawrence, J. B. (2006). The X chromosome is organized into a gene-rich outer rim and an internal core containing silenced nongenic sequences. *Proc. Natl. Acad. Sci. USA* **103**, 7688-7693.

Duret, L., Chureau, C., Samain, S., Weissenbach, J. and Avner, P. (2006). The Xist RNA gene evolved in eutherians by pseudogenization of a protein-coding gene. *Science* **312**, 1653-1655.

Gartler, S. M. and Riggs, A. D. (1983). Mammalian X-chromosome inactivation. *Annu. Rev. Genet.* **17**, 155-190.

Hadjantonakis, A. K., Gertsenstein, M., Ikawa, M., Okabe, M. and Nagy, A. (1998). Non-invasive sexing of preimplantation stage mammalian embryos. *Nat. Genet.* **19**, 220-222.

Hall, L. L., Byron, M., Sakai, K., Carrel, L., Willard, H. F. and Lawrence, J. B. (2002). An ectopic human XIST gene can induce chromosome inactivation in postdifferentiation human HT-1080 cells. *Proc. Natl. Acad. Sci. USA* **99**, 8677-8682.

Hamazaki, T., Kehoe, S. M., Nakano, T. and Terada, N. (2006). The Grb2/Mek pathway represses Nanog in murine embryonic stem cells. *Mol. Cell. Biol.* **26**, 7539-7549.

Huynh, K. D. and Lee, J. T. (2003). Inheritance of a pre-inactivated paternal X chromosome in early mouse embryos. *Nature* **426**, 857-862.

Kalantry, S., Mills, K. C., Yee, D., Otte, A. P., Panning, B. and Magnuson, T. (2006). The Polycomb group protein Eed protects the inactive X-chromosome from differentiation-induced reactivation. *Nat. Cell Biol.* **8**, 195-202.

Kalantry, S., Purushothaman, S., Bowen, R. B., Starmer, J. and Magnuson, T. (2009). Evidence of Xist RNA-independent initiation of mouse imprinted X-chromosome inactivation. *Nature* **460**, 647-651.

Kay, G. F., Penny, G. D., Patel, D., Ashworth, A., Brockdorff, N. and Rastan, S. (1993). Expression of Xist during mouse development suggests a role in the initiation of X chromosome inactivation. *Cell* **72**, 171-182.

Lee, J. T., Davidow, L. S. and Warshawsky, D. (1999). Tsix, a gene antisense to Xist at the X-inactivation centre. *Nat. Genet.* **21**, 400-404.

Lyon, M. F. (1961). Gene action in the X-chromosome of the mouse (Mus musculus L.). *Nature* **190**, 372-373.

Lyon, M. F. (1998). X-chromosome inactivation: a repeat hypothesis. *Cytogenet. Cell Genet.* **80**, 133-137.

Mak, W., Nesterova, T. B., de Napoles, M., Appanah, R., Yamanaka, S., Otte, A. P. and Brockdorff, N. (2004). Reactivation of the paternal X chromosome in early mouse embryos. *Science* **303**, 666-669.

Marahrens, Y., Panning, B., Dausman, J., Strauss, W. and Jaenisch, R. (1997). Xist-deficient mice are defective in dosage compensation but not spermatogenesis. *Genes Dev.* **11**, 156-166.

Namekawa, S. H., Payer, B., Huynh, K. D., Jaenisch, R. and Lee, J. T. (2010). Two-step imprinted X inactivation: repeat versus genic silencing in the mouse. *Mol. Cell. Biol.* **30**, 3187-3205.

Navarro, P., Chambers, I., Karwacki-Neisius, V., Chureau, C., Morey, C., Rougeulle, C. and Avner, P. (2008). Molecular coupling of Xist regulation and pluripotency. *Science* **321**, 1693-1695.

Nichols, J., Silva, J., Roode, M. and Smith, A. (2009). Suppression of Erk signalling promotes ground state pluripotency in the mouse embryo. *Development* **136**, 3215-3222.

Okamoto, I., Otte, A. P., Allis, C. D., Reinberg, D. and Heard, E. (2004). Epigenetic dynamics of imprinted X inactivation during early mouse development. *Science* **303**, 644-649.

Patrat, C., Okamoto, I., Diabangouaya, P., Vialon, V., Le Baccon, P., Chow, J. and Heard, E. (2009). Dynamic changes in paternal X-chromosome activity during imprinted X-chromosome inactivation in mice. *Proc. Natl. Acad. Sci. USA* **106**, 5198-5203.

Pawson, T. and Scott, J. D. (1997). Signaling through scaffold, anchoring, and adaptor proteins. *Science* **278**, 2075-2080.

Penny, G. D., Kay, G. F., Sheardown, S. A., Rastan, S. and Brockdorff, N. (1996). Requirement for Xist in X chromosome inactivation. *Nature* **379**, 131-137.

Plath, K., Mlynarczyk-Evans, S., Nusinow, D. A. and Panning, B. (2002). Xist RNA and the mechanism of X chromosome inactivation. *Annu. Rev. Genet.* **36**, 233-278.

Plusa, B., Piliszek, A., Frankenberg, S., Artus, J. and Hadjantonakis, A. K. (2008). Distinct sequential cell behaviours direct primitive endoderm formation in the mouse blastocyst. *Development* **135**, 3081-3091.

Rens, W., Wallduck, M. S., Lovell, F. L., Ferguson-Smith, M. A. and Ferguson-Smith, A. C. (2010). Epigenetic modifications on X chromosomes in marsupial and monotreme mammals and implications for evolution of dosage compensation. *Proc. Natl. Acad. Sci. USA* **107**, 17657-17662.

Sarma, K., Levasseur, P., Aristarkhov, A. and Lee, J. T. (2010). Locked nucleic acids (LNAs) reveal sequence requirements and kinetics of Xist RNA localization to the X chromosome. *Proc. Natl. Acad. Sci. USA* **107**, 22196-22201.

Sheardown, S. A., Duthie, S. M., Johnston, C. M., Newall, A. E., Formstone, E. J., Arkell, R. M., Nesterova, T. B., Alghisi, G. C., Rastan, S. and Brockdorff, N. (1997). Stabilization of Xist RNA mediates initiation of X chromosome inactivation. *Cell* **91**, 99-107.

Silva, J., Mak, W., Zvetkova, I., Appanah, R., Nesterova, T. B., Webster, Z., Peters, A. H., Jenuwein, T., Otte, A. P. and Brockdorff, N. (2003). Establishment of histone h3 methylation on the inactive X chromosome requires transient recruitment of Eed-Enx1 polycomb group complexes. *Dev. Cell* **4**, 481-495.

Silva, J., Nichols, J., Theunissen, T. W., Guo, G., van Oosten, A. L., Barrandon, O., Wray, J., Yamanaka, S., Chambers, I. and Smith, A. (2009). Nanog is the gateway to the pluripotent ground state. *Cell* **138**, 722-737.

Simon, J. A. and Kingston, R. E. (2009). Mechanisms of polycomb gene silencing: knowns and unknowns. *Nat. Rev. Mol. Cell Biol.* **10**, 697-708.

Solter, D. and Knowles, B. B. (1975). Immunosurgery of mouse blastocyst. *Proc. Natl. Acad. Sci. USA* **72**, 5099-5102.

Takagi, N. and Sasaki, M. (1975). Preferential inactivation of the paternally derived X chromosome in the extraembryonic membranes of the mouse. *Nature* **256**, 640-642.

West, J. D., Frels, W. I., Chapman, V. M. and Papaioannou, V. E. (1977). Preferential expression of the maternally derived X chromosome in the mouse yolk sac. *Cell* **12**, 873-882.